ACS APPLIED MATERIALS & INTERFACES

Research Article

www.acsami.org

Facial Layer-by-Layer Engineering of Upconversion Nanoparticles for Gene Delivery: Near-Infrared-Initiated Fluorescence Resonance Energy Transfer Tracking and Overcoming Drug Resistance in Ovarian Cancer

Min Lin,[*,†,‡,§] Yan Gao,[†] Thomas J. Diefenbach,[∥] Jacson K. Shen,[†] Francis J. Hornicek,[†] Yong Il Park,[⊥,#] Feng Xu,[‡,§] Tian Jian Lu,[‡,§] Mansoor Amiji,[■] and Zhenfeng Duan[*,†]

[†]Center for Sarcoma and Connective Tissue Oncology and [⊥]Center for Systems Biology, Massachusetts General Hospital, Harvard Medical School, Boston, Massachusetts 02114, United States

[‡]The Key Laboratory of Biomedical Information Engineering, Ministry of Education, School of Life Science and Technology, and [§]Bioinspired Engineering and Biomechanics Center (BEBC), Xi'an Jiaotong University, Xi'an 710049, P.R. China

[∥]Ragon Institute of MGH, Massachusetts Institute of Technology (MIT) and Harvard University, Boston, Massachusetts 02139, United States

[#]School of Chemical Engineering, Chonnam National University, Gwangju 61186, Republic of Korea

[■]Department of Pharmaceutical Sciences, School of Pharmacy, Northeastern University, Boston, Massachusetts 02115, United States

Supporting Information

ABSTRACT: Development of multidrug resistance (MDR) contributes to the majority of treatment failures in clinical chemotherapy. We report facial layer-by-layer engineered upconversion nanoparticles (UCNPs) for near-infrared (NIR)-initiated tracking and delivery of small interfering RNA (siRNA) to enhance chemotherapy efficacy by silencing the MDR1 gene and resensitizing resistant ovarian cancer cells to drug. Layer-by-layer engineered UCNPs were loaded with MDR1 gene-silencing siRNA (MDR1-siRNA) by electrostatic interaction. The delivery vehicle enhances MDR1-siRNA cellular uptake, protects MDR1-siRNA from nuclease degradation, and promotes endosomal escape for silencing the MDR gene. The intrinsic photon upconversion of UCNPs provides an unprecedented opportunity for monitoring intracellular attachment and release of MDR1-siRNA by NIR-initiated fluorescence resonance energy transfer occurs between donor UCNPs and acceptor fluorescence dye-labeled MDR1-siRNA. Enhanced chemotherapeutic efficacy in vitro was demonstrated by cell viability assay. The developed delivery vehicle holds great potential in delivery and imaging-guided tracking of therapeutic gene targets for effective treatment of drug-resistant cancers.

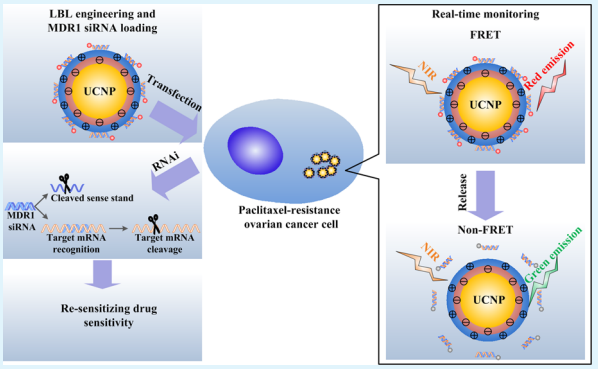

KEYWORDS: *upconversion nanoparticles, gene delivery, FRET, gene knockdown, drug sensitivity*

1. INTRODUCTION

Cancer is the second leading health issue. There were over 1.6 million new cases along with nearly 600,000 deaths in the United States in 2014.[1] As the fifth leading cause of cancer deaths in women,[2] ovarian cancer is initially responsive to anticancer chemotherapeutic agents.[3,4] However, the development of multidrug resistance (MDR) contributes to the majority of treatment failures in current cancer chemotherapy. It is estimated that 50−75% of patients suffer from recurrent/incurable ovarian cancer after initial chemotherapy.[5] Thus, development of new strategies for the treatment of various cancers with drug resistance is of vital importance.

The best known MDR mechanism involves the overexpression of P-glycoprotein (P-gp), a member of the ATP-binding cassette (ABC) transporter family of transmembrane proteins.[6] P-gp acts as a drug efflux pump to efflux chemotherapeutic drugs out of the cell, and thereby contributes to MDR by keeping the intracellular drug concentration at a low level. P-gp therefore is a promising target to overcome MDR.[7−9] With the discovery of RNA interference (RNAi) in 1998,[10] small interfering RNA (siRNA) has emerged as a promising tool for silencing MDR relevant gene expression, paving the way for resensitizing MDR cancer cells to chemotherapeutic drugs.[11] Successful RNAi relies heavily on

Received: December 1, 2016
Accepted: February 8, 2017
Published: February 8, 2017

DOI: 10.1021/acsami.6b15321
ACS Appl. Mater. Interfaces XXXX, XXX, XXX−XXX

delivery of siRNA into the cytoplasm, while being protected from enzymatic digestion and allowing sufficient endosome escape.[12]

Recent advances in nanotechnology that provide nanoparticle-based multifunctional probe for cellular imaging[13] and delivery platforms for gene delivery have attracted increasing attention.[14] Various nanoparticles, including quantum dots,[15] magnetic nanoparticles,[16] gold nanoparticles,[17] and polymeric nanoparticles,[18] have been engineered to effectively deliver genes into cells. Effective delivery, tracking, and localization of a gene during the transfection process are of vital importance to understand the intracellular fate of genes (e.g., cellular uptake, biostability, and dissociation). Understanding the transfection process will help optimize transfection efficiency by better design of nanoparticle-based delivery platforms.[19] Most nanoparticle-based delivery platforms apply UV/short visible light as the excitation source for tracking applications, which however suffer from poor tissue penetration depth and phototoxicity, leading to limited therapeutic effect.[20,21]

Upconversion nanoparticles (UCNPs) emit visible lights by near-infrared (NIR) excitation.[22,23] In particular, low photoenergy and deep tissue penetration of NIR potentiate advantages, including non-photodamage, non-autofluorescence, non-photobleaching, and deep tissue reaching.[24−29] UCNPs have thus been intensively studied for gene delivery and tracking,[30−36] and have been constructively reviewed.[37] However, despite accumulating work demonstrating the application of UCNPs for gene delivery and tracking, the possibility of using UCNPs in gene delivery for the treatment of MDR cancer cells and simultaneously tracking the intracellular fate of genes has yet to be explored.

In this study, we report a novel UCNP-based gene delivery platform for delivering MDR1-siRNA to paclitaxel-resistant ovarian cancer cells to resensitize the cells to paclitaxel, while simultaneously tracking the intracellular fate of MDR1-siRNA using sensitive and straightforward fluorescence resonance energy transfer (FRET) technique. The synthesized $NaYF_4$:Yb,Er UCNPs were surface-functionalized using facial layer-by-layer coating of poly(acrylic acid) (PAA) and polyethylenimine (PEI) counter charged polymers. The positively charged PEI layer is able to condense MDR1-siRNA for gene delivery. NIR-initiated FRET phenomenon occurred between the UCNP donor and the labeled MDR1-siRNA acceptor, which was used to track MDR1-siRNA for intracellular uptake, biostability, and dissociation from the delivery platform.

2. MATERIALS AND METHODS

Materials. The MDR ovarian cancer cell line OVCAR8TR used in this study has been well-characterized and routinely cultured as previously described.[38−40] Unlabeled MDR1-siRNA was purchased from Life Technologies Corporation (Carlsbad, CA). MDR1-siRNA was labeled with Cy3 from the Lable ITsiRNA tracker intracellular localization kit (Mirus Bio LLC, Madison, WI). MTT (3(4,5-dimethylthiazol-2-yl)-2,5-diphenyl tetrazolium bromide) reagent, mouse antihuman β-actin monoclonal antibody, and mouse antihuman P-gp monoclonal antibody were purchased from Sigma-Aldrich (St. Louis). 10× RIPA lysis buffer and complete protease inhibitor cocktail tablets were used as the manufacturer suggested. Protein assay reagents and NuPAGE 4−12% Bis-Tris Gel utilized in the Western blot were acquired from Bio-Rad (Hercules, CA) and Life Technologies, respectively. Paclitaxel was obtained from the pharmacy at the Massachusetts General Hospital. SpectraMax Microplate Spectrophotometer (Molecular Devices LLC, Sunnyvale, CA) and OdysseyCLx (LI-COR Biosciences, Lincoln, NE) were used in the current study.

Preparation of UCNP, UCNP/PAA, and UCNP/PAA/PEI. $NaYF_4$:Yb,Er UCNPs were prepared using the thermal decomposition method described by our previous studies.[41,42] To synthesis β-$NaYF_4$:Er/Yb, $YCl_3{\cdot}6H_2O$ (0.8 mmol), $YbCl_3{\cdot}6H_2O$ (0.18 mmol), and $ErCl_3{\cdot}6H_2O$ (0.02 mmol) were dissolved in 2 mL of deionized (DI) water. The mixture was then added to a flask filling with 15 mL of 1-octadecene and 7.5 mL of oleic acid. The mixture was then magnetically stirred at room temperature (RT) and was heated to 120 °C afterward. The temperature rose to 160 °C and was maintained for 1 h to get rid of water under Ar protection. Methanol solution of NH_4F and NaOH was injected into the mixture when cooling down to RT. The mixture was heated to 280 °C after methanol evaporation. After 1.5 h, the mixture was cooled down to RT. The final precipitation was washed using cyclohexane and ethanol three times. The pellet was redispersed in cyclohexane. Surface modification of UCNPs using poly(acrylic acid) (PAA) was realized by a ligand exchange method. The pellet was collected and was finally redispersed in 1 mL of DI water. An appropriate amount of 25 KD (molecular weight) polyethylenimine (PEI) was dissolved into DI water with a PEI concentration of 100 mg/mL. UCNP/PAA solution (1 mg/mL) was added dropwise into a vial containing the PEI solution (100 mg/mL). The solution was magnetically stirred and kept overnight. The pellet was collected, washed, and redispersed in 1 mL of DI water. The core UCNP concentration does not change after layer-by-layer assembly of PAA or PEI considering the negligible mass loss of the pellet during washing steps. Therefore, the concentration of UCNP/PAA or UCNP/PAA/PEI was taken as the same as the concentration of the core UCNP.

The X-ray diffraction patterns of UCNPs was characterized using an XRD-7000 diffractometer. Transmission electron microscopy (TEM) images of nanoparticles were taken by a JEOL JEM-1000 instrument (JEOL Ltd., Tokyo, Japan). Zeta potential, size distributions, and upconversion spectra of UCNP, UCNP/PAA, and UCNP/PAA/PEI were obtained by a Nano-ZS90 nanoparticle analyzer (Malvern Instruments Ltd.) and a fluorescence spectrophotometer (Quanta Master TM40) with external 980 nm laser diode, respectively. Fourier transform infrared (FTIR) spectra were obtained using PerkinElmer 2000 instrument. Thermogravimetric analysis (TGA) was performed on a Diamond TG/DTA (PerkinElmer).

Preparation of Gene UCNP/PAA/PEI Complex and Loading Efficiency Assay. An appropriate amount of UCNP/PAA/PEI was mixed with GFP plasmid DNA in DI water at different weight ratios. The mixture was incubated for 60 min at RT and was then subjected to gel electrophoresis (4% agarose). Quantitative assessment of the encapsulation efficiency and loading capacity were evaluated by PicoGreen assay.

siRNA Protection and in Vitro Release. The UCNP/PAA/PEI/MDR1-siRNA complexes with UCNP/PAA/PEI to MDR1-siRNA weight ratio of 3:1 were incubated with an equal volume of RNase (40 μg/mL) at room temperature for 10, 30, 60, 90, and 120 min, respectively. The samples were incubated at 80 °C for 5 min to cease nuclease activity. Heparin was then added to dissociate MDR1-siRNA from UCNP/PAA/PEI. The integrity of MDR1-siRNA was examined by electrophoresis (56 V for 1 h) on a 4% agarose gel. To evaluate the stability of the UCNP/PAA/PEI/MDR1-siRNA complexes, we performed heparin disassociation assay. The UCNP/PAA/PEI/MDR1-siRNA complexes were prepared at the UCNP/PAA/PEI to siRNA weight ratio of 3:1, and were then incubated with different amounts of heparin (heparin-to-siRNA weight ratio of 0, 2, 4, 6, 8, and 10) at room temperature for 30 min, respectively. siRNA release was visualized by electrophoresis on 4% agarose gel.

Cell Culture and Incubation Conditions. OVCAR8TR cells were cultured using RPMI1640 containing 10% FBS (fetal bovine serum) and 1% penicillin/streptomycin at 37 °C in a CO_2 atmosphere with humidity of 5%.

In Vitro Gene Transfection. Appropriate amounts of MDR1-siRNA and nanoparticles were each separately diluted in 50 μL of FBS and antibiotic-free medium. After vortexing, nanoparticles were mixed

DOI: 10.1021/acsami.6b15321
ACS Appl. Mater. Interfaces XXXX, XXX, XXX−XXX

with the MDR1-siRNA and incubated for 1 h at room temperature before being added into the wells.

In Vitro Imaging. Cells were visualized on a Nikon Eclipse Ti−U fluorescence microscope (Nikon Instruments, Inc., Melville, NY) equipped with a SPOT RT digital camera (Diagnostic Instruments, Inc., Sterling Heights, MI). FRET-based images were captured using a two-photon laser scanning microscope (Ultima In Vitro by Bruker Nano Corporation) equipped with two Mai Tai HP DeepSee lasers (Spectra Physics) tunable from 690 to 1040 nm. The microscope used was an Axio Examiner (Zeiss MicroImaging Inc.) equipped with a 40× Zeiss Plan-Apochromat 1.0 NA UV-IR water immersion objective.

Western Blotting Analysis. Protein lysates were extracted by using 1× RIPA lysis buffer plus complete protease inhibitor cocktail tablets. The protein concentrations were evaluated by a SpectraMax Microplate Spectrophotometer. Details can be found in our previous publication.[40]

In Vitro Cell Viability Assay. Proliferation ability of the cells and cytotoxicity of paclitaxel after nanoparticle transfection were assessed by 3-(4,5)-dimethylthiahiazo(-z-y1)-3,5-di-phenytetrazoliumromide (MTT) assay. 2 $\times 10^3$ OVCAR8TR cells per well were seeded into 96-well microplates. The cells were changed to regular medium after incubating with nanoparticle MDR1-siRNA for 6 h, and then exposed to different concentrations of paclitaxel. After 4-day incubation with a series of concentrations of paclitaxel, 20 μL of MTT was added. The samples were incubated for 4 h at 37 °C and 5% CO_2 humidified atmosphere. Acid-isopropanol was used to solubilize the intracellular formazan crystals. The absorbance of the samples was characterized using a SpectraMax Microplate Spectrophotometer at 490 nm and normalized to the value of untreated cells.

3. RESULTS AND DISCUSSION

Fabrication and Characterization of $NaYF_4$:Yb,Er/PAA/PEI Nanoparticles. In this study, we engineered $NaYF_4$:Yb,Er UCNP-based gene delivery system for NIR-initiated FRET tracking, as well as for overcoming drug resistance in ovarian cancer. Figure 1a illustrates schematically the layer-by-layer assembly process. UCNPs were fabricated using the thermal decomposition method in an oleic acid (OA) solution. To make the synthesized UCNPs soluble in an aqueous solution, a ligand exchange method was carried out to exchange the hydrophobic OA ligand with hydrophilic PAA following our published procedures.[38,39] The presence of the negatively charged PAA layer facilitates further coating of positively charged PEI via electrostatic interaction. The positively charged PEI layer condenses the negatively charged gene to form a stable complex. PEI is a cationic polymer composed of repeating units of amine groups, which facilitates endosomal escape due to the proton sponge effect.[43]

XRD patterns show that all of the diffraction peaks can be ascribed to the hexagonal structure of $NaYF_4$ (JCPDS no. 16-0334), suggesting that $NaYF_4$:Yb,Er exhibits a pure hexagonal phase (Figure S1 of the Supporting Information). TEM images show that the synthesized UCNPs are monodispersed nanoparticles with an average diameter of about 39 nm (Figure 1b, Figure S2a). A core−shell structure could be identified after PAA coating (Figure 1c). The PAA layer thickness was estimated to be about 5 nm and the average size of UCNP/PAA was about 45 nm (Figure S2b). After the final PEI coating, the layer thickness slightly increased to about 7 nm and the average size of UCNP/PAA/PEI was about 47 nm (Figure 1d, Figure S2c). No aggregation was observed after layer-by-layer assembly of PAA and PEI layers. The hydrodynamic sizes of UCNP/PAA and UCNP/PAA/PEI were analyzed by DSL (Figure 1e). Measured size distributions revealed that both UCNP/PAA and UCNP/PAA/PEI were uniformly coated and well dispersed in an aqueous solution. The hydrodynamic size

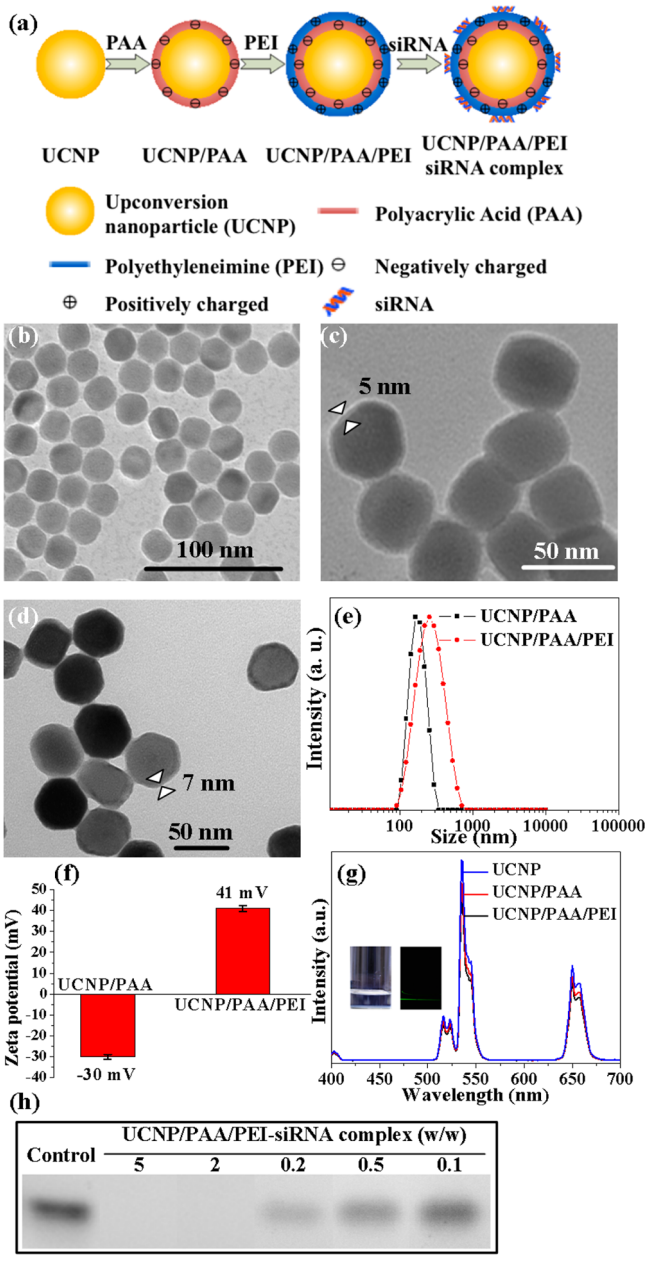

Figure 1. Preparation of UCNP-based gene delivery system. (a) Schematic illustration for the preparation of layer-by-layer assembled UCNP/PAA/PEI/siRNA complex. Transmission electron microscopic images of (b) naked UCNPs showing an average diameter of 40 nm, (c) PAA-coated UCNPs, showing layer thickness of ∼5 nm, and (d) PAA/PEI-coated UCNPs, showing dense inner layer and loose outer layer with a total thickness of ∼7 nm. Arrows indicate the polyelectrolyte layers of PAA and PEI. (e) Dynamic light scattering measured diameter in DI water for UCNP/PAA and UCNP/PAA/PEI. (f) Zeta-potential analysis of UCNP/PAA and UCNP/PAA/PEI in DI water. Zeta potential was measured three times. (g) Upconversion emission spectra of UCNP samples after PAA and PEI polymers coatings under 980 nm excitation recorded at the same UCNP concentration. The inset shows photographs of the UCNP/PAA/PEI in DI water under ambient light (left) or exposed to 980 nm laser (right). (h) Agarose gel electrophoresis of bare MDR1-siRNA (control) and MDR1-siRNA mixed with UCNP/PEI at different weight ratios.

of UCNP/PAA was about 168 nm; additional PEI coating increased the hydrodynamic size to about 235 nm. It should be

DOI: 10.1021/acsami.6b15321
ACS Appl. Mater. Interfaces XXXX, XXX, XXX−XXX

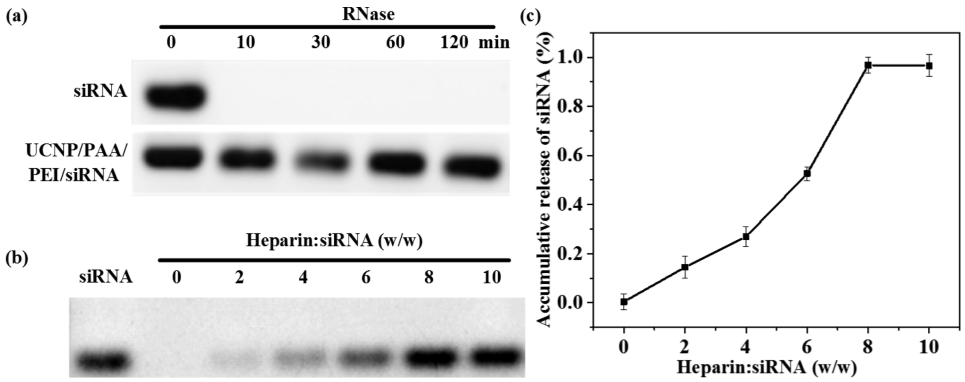

Figure 2. Stability and releasing kinetics of UCNP/PAA/PEI/siRNA complex. (a) Resistance of siRNA in UCNP/PAA/PEI/siRNA complex against nuclease degradation. (b) Gel images for the stability of UCNP/PAA/PEI/siRNA complex against polyanion (heparin) exchange reaction with different weight ratio of heparin over siRNA. (c) Quantitative analysis of accumulative release of siRNA. All UCNP/PAA/PEI/siRNA complexes were prepared at the UCNP/PAA/PEI to MDR1-siRNA weight ratio of 3:1.

noted that the hydrodynamic size measured by DLS is larger than that determined by TEM. The difference in diameter can be explained by the fact that hydrodynamic size is determined by analyzing and calculating from the dynamic diffusion property of UCNP/PAA and UCNP/PAA/PEI in a hydrated state. The appearance of a single peak for both UCNP/PAA and UCNP/PAA/PEI suggests relatively narrow size distribution and their well dispersion in the solution.[30,44] This is also confirmed by TEM results in Figure 1c,d.

To further confirm the formation of layer-by-layer charged polymer layers on the surface of UCNPs, we measured the surface charge with a zeta-potential analyzer. Figure 1f displays the zeta-potentials of UCNPs with different polymer layers. The zeta-potential of UCNPs with negatively charged PAA coating (UCNP/PAA) was measured as −30 mV, which jumped to +41 mV after positive PEI coating (UCNP/PAA/PEI). These discrete zeta-potential values alternating between negative for UCNP/PAA and positive for UCNP/PAA/PEI indicate successful layer-by-layer assembly of PAA and PEI polymers with counter charge.

FTIR spectroscopy measurements were performed to identify the presence of ligands on UCNPs (Figure S3a). The UCNPs and UCNP/PAA samples exhibited a broad band at approximately 3432 cm^{-1}, corresponding to the O−H stretching vibration. The 2925 and 2851 cm^{-1} transmission bands in the UCNPs sample nonresponse to the asymmetric and symmetric stretching vibrations of the −CH2− in alkyl chain, and 1567 and 1463 cm^{-1} transmission bands, are associated with the asymmetric and symmetric stretching vibrations of carboxylate anions.[45] For UCNP/PAA sample, the shoulders at 2925 and 2851 cm^{-1} associated with the asymmetrical stretching of the $-CH_2-$ groups are reduced and the appearance of a strong band at 1718 cm^{-1} as a result of the vibrations of the −COOH group suggest the replacement of PAA with OA on the surface of UCNPs.[25,45] The peak at 3176 cm^{-1} in the UCNP/PAA/PEI sample comes from NH_2 and −COOH interaction. The peak at 1502 cm^{-1} contributes to NH_3^+ symmetric deformation. This confirms the coating of PEI layer.[46]

TGA results further confirm layer-by-layer construction of UCNPs (Figure S3b). In the whole temperature range, the relative weight loss for UCNPs is approximately 6%, assigned to the decomposition of OA coating and evaporation of adsorbed. For UCNP/PAA, PAA began to degrade at about 200 °C. A strong primary mass loss between 200 and 500 °C could be observed and the final weight loss is ∼11%. The significant decomposition of UCNP/PAA/PEI begins at about 200 °C. The thermal decomposition of PEI resulted in additional weight loss of ∼4%.

Upconversion luminescence spectra of UCNP, UCNP/PAA, and UCNP/PAA/PEI at the same UCNP concentration are presented in Figure 1g. Upon 980 nm near-infrared laser excitation, the three samples exhibited similar emission patterns, with major emission peaks at around 530 and 650 nm. The highest emission intensity was identified from the UCNPs sample. After PAA coating, the peak green emission intensity reduced to 88% as compared with that of the original UCNPs. The subsequent PEI coating further reduced the green emission peak intensity to 80% as compared with that of the original UCNPs.

Characterization of Gene Loading Capacity and Intracellular Delivery. To study the siRNA loading capability of UCNP/PAA/PEI, we performed gel electrophoresis by mixing UCNP/PAA/PEI with siRNA at different weight/weight (w/w) ratios (Figure 1h). UCNP/PAA/PEI could efficiently bind siRNA as evidenced by significant retardation of siRNA migration in the gel electrophoresis at a w/w ratio above 0.2. Quantitative examination of siRNA encapsulation efficiency and loading capacity was assessed by PicoGreen assay. The siRNA encapsulation efficiency (AE) and loading capacity (LC) and were calculated from eqs 1 and 2 indicated below,[47]

$$\mathrm{AE} = (A - B)/A \times 100 \quad (1)$$

$$\mathrm{LC} = (A - B)/C \times 100 \quad (2)$$

where A is the total amount of siRNA, B is the free amount of siRNA, and C is the nanoparticles weight. The encapsulation efficiency and loading capacity were separately determined to be 97.264% and 34.1% (calculated from Figure S4). Besides siRNA, loading of GFP-expressing plasmid DNA by UCNP/PAA/PEI was also demonstrated, as shown in Figure S5.

Protection of siRNA Integrity and Binding/Releasing. We further evaluated the capability of UCNP/PAA/PEI delivery platform in the protection of MDR1-siRNA integrity against nuclease degradation. To this end, naked MDR1-siRNA and UCNP/PAA/PEI/MDR1-siRNA complex were separately mixed with RNase with different time durations. The electrophoresis results indicate rapid degradation of naked MDR1-siRNA in RNase solution for less than 10 min (Figure 2a), whereas approximately 100% of the MDR1-siRNA

DOI: 10.1021/acsami.6b15321
ACS Appl. Mater. Interfaces XXXX, XXX, XXX−XXX

encapsulated in UCNP/PAA/PEI was released as evidenced by bright bands indicate that the delivery platform protected MDR1-siRNA against nuclease attack.

The kinetics of dissociation of MDR1-siRNA from UCNP/PAA/PEI was accessed by heparin competition assay (Figure 2b). Accumulative release of MDR1-siRNA was calculated by normalizing the band intensity. UCNP/PAA/PEI/MDR1-siRNA complex began to release MDR1-siRNA at the heparin/MDR1-siRNA ratio of 2 (Figure 2c). At heparin/MDR1-siRNA weight ratio of 6, 50% MDR1-siRNA released from UCNP/PAA/PEI/MDR1-siRNA complex (Figure 2c). These results suggest a distinct binding affinity between MDR1-siRNA and UCNP/PAA/PEI.

A high siRNA uptake level is required for efficient siRNA-regulated gene silencing.[48] To study the role of UCNP/PAA/PEI delivery of MDR1-siRNA into the cytoplasm of OVCAR8TR cells, we employed a fluorescence microscope to observe the presence of Cy3-labeled MDR1-siRNA (red fluorescence) in the cytoplasm (Figure 3). Compared with the

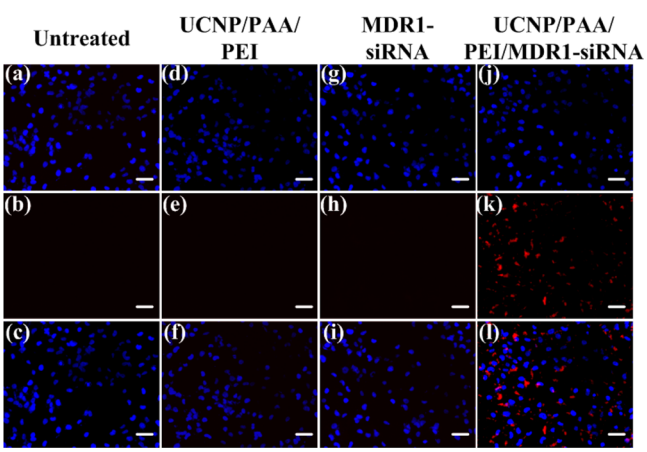

Figure 3. Fluorescence microscope imaging of OVCAR8TR cells after 24 h of the initiation of transfection with UCNP/PAA/PEI, MDR1-siRNA, and UCNP/PAA/PEI/MDR1-siRNA. (a) DAPI emission of untreated group. (b) Imaging under excitation wavelength of 530−550 nm. (c) Merged image of (a) and (b). (d) DAPI emission of OVCAR8TR cells treated with UCNP/PAA/PEI. (e) Imaging under excitation wavelength of 530−550 nm. (f) Merged image of (d) and (e). (g) DAPI emission of OVCAR8TR cells treated with MDR1-siRNA. MDR1-siRNA were labeled with Cy3. (h) Imaging under excitation wavelength of 530−550 nm. (i) Merged image of (g) and (h). (j) DAPI emission of OVCAR8TR cells treated with UCNP/PAA/PEI/MDR1-siRNA complex. MDR1-siRNA were labeled with Cy3. (k) Imaging under excitation wavelength of 530−550 nm showing red fluorescence from labeled MDR1-siRNA. (l) Merged image of (j) and (k). The bar represents 50 μm.

transfection of a naked siRNA solution, cellular uptake of labeled MDR1-siRNA loaded onto UCNP/PAA/PEI was significantly enhanced as evidenced by the detected red fluorescence signal. Co-localization images taken from different channels indicated that UCNP/PAA/PEI facilitated siRNA internalization by endocytosis pathways. Besides OVCAR8TR cells, we also demonstrated successful transfection of MDR1-siRNA into U2OS cells using the presently developed delivery platform (Figure S6). The flexibility of this delivery platform in delivering GFP plasmid DNA into U2OS cells and Let-7 miRNAs into OVCAR8TR cells was further evidenced by Figures S7 and S8.

FRET-Based Imaging-Guided Monitoring of Intracellular Attachment and Release of Gene from Delivery Platform. FRET features nonradiative energy transfer from a donor fluorophore to an acceptor fluorophore when the donor and the acceptor are in close proximity.[42,49] FRET has been widely applied as a noninvasive spectroscopic method for assessing the association and disassociation of bimolecular complex.[50] We therefore employed NIR-initiated, sensitive, and straightforward FRET technology to noninvasively track MDR1-siRNA transfection processes, including cellular uptake, biostability, association, and disassociation from the delivering platform. To this end, we constructed layer-by-layer assembled UCNP/PAA/PEI acting simultaneously as a gene carrier and a donor fluorophore for NIR to initiate FRET tracking.

To enable FRET, MDR1-siRNA was prelabeled with Cy3 dye, a red fluorescence dye. Spectral overlap between UCNPs with emission peak at 538 nm and labeled MDR1-siRNA with absorption peak at 547 nm facilitated nonradiative energy transfer between the FRET pair (Figure S9a). To demonstrate the formation of the FERT pair, we added a different amount of Cy3 labeled MDR1-siRNA in to UCNP/PAA/PEI solution with UCNP/PAA/PEI to MDR1-siRNA weight ratio of 5:1, 4:1, 3:1, and 2:1, respectively, and followed by incubation as well as fluorescence spectrum scanning under an external 980 nm cw laser excitation. We found that the upconversion fluorescence of UCNP/PAA/PEI was gradually quenched as the amount of Cy3-labeled MDR1-siRNA was increased (Figure S9b).

The FRET distances were estimated to be R_0(min) = 2.52 nm or R_0(max) = 3.71 nm considering that the quantum yield of UCNPs falls between 0.001 and 0.01.[51] The FRET efficiency was estimated to be η(min) = 0.5% and η(max) = 3%.[52] The detailed calculation processes could be found in the Supporting Information.

To confirm NIR-initiated FRET tracing of siRNA, we transfected the constructed UCNP/PAA/PEI/siRNA FRET pair into OVCAR8TR cells and imaged at 3 h post-transfection, as shown in Figure 4a−e. Upon 980 nm excitation, green upconversion emission from the green channel was observed in the cytoplasm (Figure 4d), suggesting the presence of UCNPs in the cytoplasm. When the cell sample was excited at 1040 nm (direct excitation of labeled MDR1-siRNA in a two-photon system), red emission from directly excited labeled MDR1-siRNA was observed, which indicated the presence of MDR1-siRNA in the cytoplasm (Figure 4b). It should be noted that the red emission upon direct excitation of labeled MDR1-siRNA after 24 h post-transfection (Figure 4b) is significantly weakened as compared to that after 3 h post-transfection (Figure 4g). This phenomenon suggests that before release from the nanoparticles, the aggregated labeled MDR1-siRNA produced strong red emission, while after 24 h post-transfection the labeled MDR1-siRNA were released from the nanoparticles. Both dye spreading and bleaching (decomposition) may contribute to the reduced red emission. A bandpass filter that allows passing through only Cy3 emission range upon 980 nm excitation was utilized. Then the red emission from labeled MDR1-siRNA recorded from the red channel was observed under 980 nm excitation, confirming the occurrence of FRET between donor UCNPs and acceptor labeled MDR1-siRNA (Figure 4c). The distribution of red emission follows a pattern similar to that of green upconversion emission. Co-localization of red and green fluorescence produces yellow color (indicated by yellow arrows in Figure

DOI: 10.1021/acsami.6b15321
ACS Appl. Mater. Interfaces XXXX, XXX, XXX−XXX

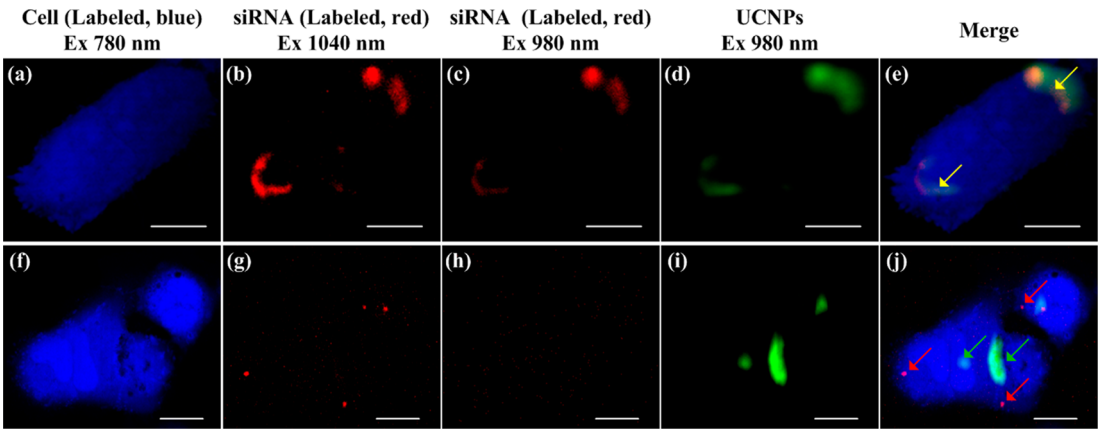

Figure 4. Two-photon imaging of OVCAR8TR cells transfected with UCNP/PAA/PEI/MDR1-siRNA complex for 3 h (a–e) and 24 h (f–j) to study the association and disassociation of MDR1-siRNA from the UCNPs-based delivery platform. (a, f) Blue emission from Celltracker Blue labeled OVCAR8TR cell. (b, g) Red emission from directly excited Cy3-labeled MDR1-siRNA. (c) FRET-induced red emission from labeled MDR1-siRNA under 980 nm excitation. (h) No emission was observed under 980 nm excitation. (d, i) Upconversion emission from UCNPs under 980 nm excitation. (e) Merged image of (c) and (d). Yellow color merged by green (emitted from UCNPs) and red (emitted from labeled MDR1-siRNA) colors is shown by yellow arrows, indicating the association of MDR1-siRNA on the UCNPs-based delivery platform. (j) Merged image of (g) and (i). MDR1-siRNA successfully disassociated from UCNP-based delivery platform as evidenced by the separation of green (green arrow) and red (red arrows) fluorescence. The bar represents 15 μm.

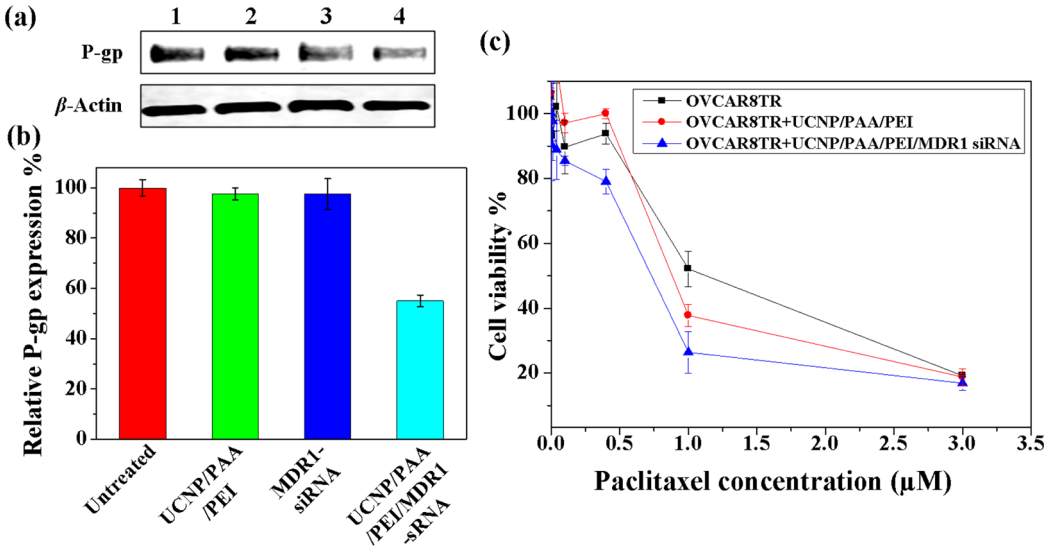

Figure 5. In vitro gene-silencing efficiency and antidrug resistance efficacy. (a) Western blot for the detection of P-gp expression in response to OVCAR8TR cells with different treatments. Lanes 1–4: Untreated, UCNP/PAA/PEI, free MDR1-siRNA, and UCNP/PAA/PEI/MDR1-siRNA complex. (b) Quantitative analysis of P-gp expression was expressed as percentage values of untreated group was performed using ImageJ software. (c) Resensitizing of OVCAR8TR cells to paclitaxel treatment. Paclitaxel-resistant ovarian cancer cells OVCAR8TR was transfected with UCNP/PAA/PEI and UCNP/PAA/PEI/MDR1-siRNA complex. Paclitaxel (with concentrations ranging between 0 and 3.0 μM) dosing was performed after 24 h of post-transfection and then the cytotoxicity was determined after 4-day incubation by the MTT assay. The MTT assay was conducted in triplicate.

4e), and thus provides strong evidence of FRET occurrence. This FRET suggests that MDR1-siRNA were delivered into cells and had not yet been released from UCNP/PAA/PEI.[31]

siRNA disassociation from the delivery platform after a prolonged incubation time was assessed by the loss of FRET (Figure 4f–j). After 24 h post-transfection, red emission from the cell sample upon direct excitation of labeled MDR1-siRNA with 1040 nm demonstrated the presence of MDR1-siRNA in the cytoplasm (Figure 4g). However, when the sample was exposed to 980 nm excitation, no emission from the red channel was observed (Figure 4h), while only green emission was observed in the green channel (Figure 4i). The missing red emission in the red channel demonstrated blocked nonradiative energy transfer between donor UCNPs and acceptor labeled MDR1-siRNA. The loss of FRET suggests the disassociation of siRNA from the delivery platform.[32] The arrow in colocalized red emission from labeled MDR1-siRNA and green emission from UCNPs (Figure 4j) show separation of red and green emission, thus confirming the disassociation of MDR1-siRNA. These images also suggest that MDR1-siRNA is delivered into the cytoplasm by UCNP/PAA/PEI and are kept intact from enzyme cleave. We further demonstrated successfully using FRET technology to noninvasively track the transfection process of Let-7 miRNAs (Figure S10). This indicates the flexibility of the present UCNP-based delivery platform for delivering different nucleic acids into cells while being able to

DOI: 10.1021/acsami.6b15321
ACS Appl. Mater. Interfaces XXXX, XXX, XXX–XXX

track their association and disassociation from the delivering platform.

In Vitro Gene Silencing Efficiency and Reversed Drug Resistance Efficacy. To evaluate the capability of the UCNP/PAA/PEI/MDR1-siRNA complex in MDR reversal for enhanced chemotherapy efficacy, we applied a siRNA targeting MDR1, the gene that encodes P-gp, which is overexpressed in the OVCAR8TR cell line. P-gp expression levels for untreated OVCAR8TR cells and cells that were treated with UCNP/PAA/PEI, free MDR1-siRNA, or UCNP/PAA/PEI/MDR1-siRNA complex was determined by Western blotting. As compared with untreated (Figure 5a, Lane 1) and UCNP/PAA/PEI (Figure 5a, Lane 2) or free MDR1-siRNA treated (Figure 5a, Lane 3) groups, significant P-gp knockdown was found with the UCNP/PAA/PEI/MDR1-siRNA complex treated group (Figure 5a Lane 4). Quantification of Western blotting results is presented in Figure 5b. Results showed that P-gp expression was reduced by about 40% for OVCAR8TR cells treated with UCNP/PAA/PEI/MDR1-siRNA complex. In contrast, UCNP/PAA/PEI or free MDR1-siRNA treatment showed no appreciable effect on P-gp expression.

We further evaluated whether the knockdown of P-gp could reverse paclitaxel resistance in OVCAR8TR cells. Cell viabilities for different cell groups treated with increasing paclitaxel concentrations were assessed by MTT assay (Figure 5c). The paclitaxel IC_{50} values of OVCAR8TR and OVCAR8TR pretreated with UCNP/PAA/PEI or UCNP/PAA/PEI/MDR1-siRNA complex was calculated to be 0.91, 0.70, and 0.59 μM, respectively. Negligible cytotoxicity (with cell viability of 97.1 $\pm$ 3.0%) was observed at a paclitaxel concentration of zero, indicating that OVCAR8TR cells tolerated well the UCNP/PAA/PEI and UCNP/PAA/PEI/MDR1-siRNA complex at the dose used in this study. After transfection of MDR1-siRNA utilizing UCNP/PAA/PEI, the IC_{50} value decreased by 1.5-fold compared with untreated OVCAR8TR cells. This result suggests that transfection with UCNP/PAA/PEI/MDR1-siRNA complex could knock down P-gp expression in paclitaxel-resistant OVCAR8TR cells, facilitating intracellular drug accumulation,[6] thereby resensitizing OVCAR8TR cells for enhanced in vitro chemotherapeutic efficacy. Thus, our results demonstrated that the UCNP/PAA/PEI nanoparticle system could successfully deliver MDR1-siRNA into cells, knock down its targeted MDR1-mRNA and P-gp, and function to reverse drug resistance in ovarian cancer in vitro.

4. CONCLUSIONS

In summary, we report the first attempt of utilizing facial layer-by-layer surface functionalized UCNPs as an efficient gene delivery platform to simultaneously delivery MDR1-siRNA to paclitaxel-resistant ovarian cancer cells and track the intracellular fate of MDR1-siRNA. Our results indicate that the UCNP/PAA/PEI/MDR1-siRNA nanocomplex enables effective gene silencing in paclitaxel-resistant ovarian cancer cells and resensitizing the cells to paclitaxel treatment. The occurrence of FRET between the UCNPs and labeled MDR1-siRNA provided real-time evidence for attachment and release of siRNA in live cells.

■ ASSOCIATED CONTENT

Supporting Information

The Supporting Information is available free of charge on the ACS Publications website at DOI: 10.1021/acsami.6b15321.

XRD pattern, size distribution analysis, FTIR/TGA analysis, PicoGreen assay, agarose gel electrophoresis assay, fluorescence microscope images of siRNA transfection, fluorescence images of GFP pDNA transfection, fluorescence microscope images of miRNA transfection, spectral overlap, FRET-induced quenching, two-photon imaging analysis, and estimation of FRET distance and efficiency (PDF)

■ AUTHOR INFORMATION

Corresponding Authors

*E-mail: minlin@xjtu.edu.cn.

*E-mail: ZDUAN@mgh.harvard.edu.

ORCID

Min Lin: 0000-0002-3259-1955

Feng Xu: 0000-0003-4351-0222

Author Contributions

M.L. and Z.F.D. conceived the project. M.L., Y.G., and T.D. performed the experiments and collected the data. M.L., Z.F.D., M.A., F.H., J.S., F.X., Y.P., and T.J.L. were involved in design and interpretation of the experiments. All authors participated in preparation of the manuscript.

Notes

The authors declare no competing financial interest.

■ ACKNOWLEDGMENTS

This study is supported in part by grants from the Gategno and Wechsler funds. Dr. Duan is supported, in part, through a grant from Sarcoma Foundation of America (SFA), a grant from National Cancer Institute (NCI)/National Institutes of Health (NIH), UO1, CA 151452, By the National Natural Science Foundation of China (11402192), and the Fundamental Research Funds for the Central Universities (2016qngz03). We thank Dr. Ralph Weissleder for his insights and support on this work.

■ REFERENCES

(1) Siegel, R.; Ma, J.; Zou, Z.; Jemal, A. Cancer Statistics, 2014. *Ca-Cancer J. Clin.* **2014**, *64*, 9−29.

(2) Siegel, R. L.; Miller, K. D.; Jemal, A. Cancer Statistics, 2015. *Ca-Cancer J. Clin.* **2015**, *65*, 5−29.

(3) Coleman, R. L.; Monk, B. J.; Sood, A. K.; Herzog, T. J. Latest Research and Treatment of Advanced-Stage Epithelial Ovarian Cancer. *Nat. Rev. Clin. Oncol.* **2013**, *10*, 211−224.

(4) Vaughan, S.; Coward, J. I.; Bast, R. C.; Berchuck, A.; Berek, J. S.; Brenton, J. D.; Coukos, G.; Crum, C. C.; Drapkin, R.; Etemadmoghadam, D.; Friedlander, M.; Gabra, H.; Kaye, S. B.; Lord, C. J.; Lengyel, E.; Levine, D. A.; McNeish, I. A.; Menon, U.; Mills, G. B.; Nephew, K. P.; Oza, A. M.; Sood, A. K.; Stronach, E. A.; Walczak, H.; Bowtell, D. D.; Balkwill, F. R. Rethinking Ovarian Cancer: Recommendations for Improving Outcomes. *Nat. Rev. Cancer* **2011**, *11*, 719−725.

(5) Herzog, T. J. Recurrent Ovarian Cancer: How Important Is It to Treat to Disease Progression? *Clin. Cancer Res.* **2004**, *10*, 7439−7449.

(6) Holohan, C.; Van Schaeybroeck, S.; Longley, D. B.; Johnston, P. G. Cancer Drug Resistance: An Evolving Paradigm. *Nat. Rev. Cancer* **2013**, *13*, 714−726.

(7) He, C.; Lu, K.; Liu, D.; Lin, W. Nanoscale Metal−Organic Frameworks for the Co-Delivery of Cisplatin and Pooled siRNAs to Enhance Therapeutic Efficacy in Drug-Resistant Ovarian Cancer Cells. *J. Am. Chem. Soc.* **2014**, *136*, 5181−5184.

(8) Duan, Z.; Zhang, J.; Ye, S.; Shen, J.; Choy, E.; Cote, G.; Harmon, D.; Mankin, H.; Hua, Y.; Zhang, Y.; Gray, N. S.; Hornicek, F. J. A-

DOI: 10.1021/acsami.6b15321
ACS Appl. Mater. Interfaces XXXX, XXX, XXX−XXX

770041 Reverses Paclitaxel and Doxorubicin Resistance in Osteosarcoma Cells. *BMC Cancer* **2014**, *14*, 681−691.
(9) He, C.; Liu, D.; Lin, W. Self-Assembled Nanoscale Coordination Polymers Carrying siRNAs and Cisplatin for Effective Treatment of Resistant Ovarian Cancer. *Biomaterials* **2015**, *36*, 124−133.
(10) Fire, A.; Xu, S.; Montgomery, M. K.; Kostas, S. A.; Driver, S. E.; Mello, C. C. Potent and Specific Genetic Interference by Double-Stranded Rna in Caenorhabditis Elegans. *Nature* **1998**, *391*, 806−811.
(11) Yhee, J. Y.; Song, S.; Lee, S. J.; Park, S.-G.; Kim, K.-S.; Kim, M. G.; Son, S.; Koo, H.; Kwon, I. C.; Jeong, J. H.; Jeong, S. Y.; Kim, S. H.; Kim, K. Cancer-Targeted MDR-1 siRNA Delivery Using Self-Cross-Linked Glycol Chitosan Nanoparticles to Overcome Drug Resistance. *J. Controlled Release* **2015**, *198*, 1−9.
(12) Tan, S. J.; Kiatwuthinon, P.; Roh, Y. H.; Kahn, J. S.; Luo, D. Engineering Nanocarriers for siRNA Delivery. *Small* **2011**, *7*, 841−856.
(13) Xu, H.; Li, Q.; Wang, L.; He, Y.; Shi, J.; Tang, B.; Fan, C. Nanoscale Optical Probes for Cellular Imaging. *Chem. Soc. Rev.* **2014**, *43*, 2650−2661.
(14) Williford, J. M.; Wu, J.; Ren, Y.; Archang, M. M.; Leong, K. W.; Mao, H. Q. Recent Advances in Nanoparticle-Mediated siRNA Delivery. *Annu. Rev. Biomed. Eng.* **2014**, *16*, 347−370.
(15) Yang, H. N.; Park, J. S.; Jeon, S. Y.; Park, W.; Na, K.; Park, K. H. The Effect of Quantum Dot Size and Poly(Ethylenimine) Coating on the Efficiency of Gene Delivery into Human Mesenchymal Stem Cells. *Biomaterials* **2014**, *35*, 8439−8449.
(16) Jiang, S.; Eltoukhy, A. A.; Love, K. T.; Langer, R.; Anderson, D. G. Lipidoid-Coated Iron Oxide Nanoparticles for Efficient DNA and siRNA Delivery. *Nano Lett.* **2013**, *13*, 1059−1064.
(17) Han, L.; Zhao, J.; Zhang, X.; Cao, W.; Hu, X.; Zou, G.; Duan, X.; Liang, X. J. Enhanced siRNA Delivery and Silencing Gold−Chitosan Nanosystem with Surface Charge-Reversal Polymer Assembly and Good Biocompatibility. *ACS Nano* **2012**, *6*, 7340−7351.
(18) Yang, X.; lyer, A. K.; Singh, A.; Choy, E.; Hornicek, F. J.; Amiji, M. M.; Duan, Z. MDR1 siRNA Loaded Hyaluronic Acid-Based Cd44 Targeted Nanoparticle Systems Circumvent Paclitaxel Resistance in Ovarian Cancer. *Sci. Rep.* **2015**, *5*, 8509.
(19) Jayakumar, M. K. G.; Bansal, A.; Huang, K.; Yao, R.; Li, B. N.; Zhang, Y. Near-Infrared-Light-Based Nano-Platform Boosts Endosomal Escape and Controls Gene Knockdown in Vivo. *ACS Nano* **2014**, *8*, 4848−4858.
(20) Cheng, L.; Wang, C.; Feng, L.; Yang, K.; Liu, Z. Functional Nanomaterials for Phototherapies of Cancer. *Chem. Rev.* **2014**, *114*, 10869−10939.
(21) Bansal, A.; Zhang, Y. Photocontrolled Nanoparticle Delivery Systems for Biomedical Applications. *Acc. Chem. Res.* **2014**, *47*, 3052−3060.
(22) Liu, Q.; Feng, W.; Li, F. Water-Soluble Lanthanide Upconversion Nanophosphors: Synthesis and Bioimaging Applications in Vivo. *Coord. Chem. Rev.* **2014**, *273*−*274*, 100−110.
(23) Lin, M.; Zhao, Y.; Wang, S.; Liu, M.; Duan, Z.; Chen, Y.; Li, F.; Xu, F.; Lu, T. Recent Advances in Synthesis and Surface Modification of Lanthanide-Doped Upconversion Nanoparticles for Biomedical Applications. *Biotechnol. Adv.* **2012**, *30*, 1551−1561.
(24) Liu, Q.; Feng, W.; Yang, T.; Yi, T.; Li, F. Upconversion Luminescence Imaging of Cells and Small Animals. *Nat. Protoc.* **2013**, *8*, 2033−2044.
(25) Liu, B.; Chen, Y.; Li, C.; He, F.; Hou, Z.; Huang, S.; Zhu, H.; Chen, X.; Lin, J. Poly(Acrylic Acid) Modification of Nd^{3+}-Sensitized Upconversion Nanophosphors for Highly Efficient Ucl Imaging and Ph-Responsive Drug Delivery. *Adv. Funct. Mater.* **2015**, *25*, 4717−4729.
(26) Yi, Z.; Li, X.; Xue, Z.; Liang, X.; Lu, W.; Peng, H.; Liu, H.; Zeng, S.; Hao, J. Remarkable Nir Enhancement of Multifunctional Nanoprobes for in Vivo Trimodal Bioimaging and Upconversion Optical/T2-Weighted Mri-Guided Small Tumor Diagnosis. *Adv. Funct. Mater.* **2015**, *25*, 7119−7129.
(27) Feng, A. L.; Lin, M.; Tian, L.; Zhu, H. Y.; Guo, H.; Singamaneni, S.; Duan, Z.; Lu, T. J.; Xu, F. Selective Enhancement of Red Emission from Upconversion Nanoparticles Via Surface Plasmon-Coupled Emission. *RSC Adv.* **2015**, *5*, 76825−76835.
(28) Xiang, J.; Xu, L.; Gong, H.; Zhu, W.; Wang, C.; Xu, J.; Feng, L.; Cheng, L.; Peng, R.; Liu, Z. Antigen-Loaded Upconversion Nanoparticles for Dendritic Cell Stimulation, Tracking, and Vaccination in Dendritic Cell-Based Immunotherapy. *ACS Nano* **2015**, *9*, 6401−6411.
(29) Lai, J.; Shah, B. P.; Zhang, Y.; Yang, L.; Lee, K.-B. Real-Time Monitoring of Atp-Responsive Drug Release Using Mesoporous-Silica-Coated Multicolor Upconversion Nanoparticles. *ACS Nano* **2015**, *9*, 5234−5245.
(30) He, L.; Feng, L.; Cheng, L.; Liu, Y.; Li, Z.; Peng, R.; Li, Y.; Guo, L.; Liu, Z. Multilayer Dual-Polymer-Coated Upconversion Nanoparticles for Multimodal Imaging and Serum-Enhanced Gene Delivery. *ACS Appl. Mater. Interfaces* **2013**, *5*, 10381−10388.
(31) Guo, H.; Idris, N. M.; Zhang, Y. Lret-Based Biodetection of DNA Release in Live Cells Using Surface-Modified Upconverting Fluorescent Nanoparticles. *Langmuir* **2011**, *27*, 2854−2860.
(32) Jiang, S.; Zhang, Y. Upconversion Nanoparticle-Based Fret System for Study of siRNA in Live Cells. *Langmuir* **2010**, *26*, 6689−6694.
(33) Wang, X.; Liu, K.; Yang, G.; Cheng, L.; He, L.; Liu, Y.; Li, Y.; Guo, L.; Liu, Z. Near-Infrared Light Triggered Photodynamic Therapy in Combination with Gene Therapy Using Upconversion Nanoparticles for Effective Cancer Cell Killing. *Nanoscale* **2014**, *6*, 9198−9205.
(34) Yang, Y.; Liu, F.; Liu, X.; Xing, B. NIR Light Controlled Photorelease of siRNA and Its Targeted Intracellular Delivery Based on Upconversion Nanoparticles. *Nanoscale* **2013**, *5*, 231−238.
(35) Jiang, S.; Zhang, Y.; Lim, K. M.; Sim, E. K. W.; Ye, L. NIR-to-Visible Upconversion Nanoparticles for Fluorescent Labeling and Targeted Delivery of siRNA. *Nanotechnology* **2009**, *20*, 155101.
(36) Jayakumar, M. K. G.; Idris, N. M.; Zhang, Y. Remote Activation of Biomolecules in Deep Tissues Using near-Infrared-to-Uv Upconversion Nanotransducers. *Proc. Natl. Acad. Sci. U. S. A.* **2012**, *109*, 8483−8488.
(37) Lin, M.; Gao, Y.; Hornicek, F.; Xu, F.; Lu, T. J.; Amiji, M.; Duan, Z. Near-Infrared Light Activated Delivery Platform for Cancer Therapy. *Adv. Colloid Interface Sci.* **2015**, *226*, 123−137.
(38) Duan, Z.; Feller, A. J.; Penson, R. T.; Chabner, B. A.; Seiden, M. V. Discovery of Differentially Expressed Genes Associated with Paclitaxel Resistance Using Cdna Array Technology: Analysis of Interleukin (Il) 6, Il-8, and Monocyte Chemotactic Protein 1 in the Paclitaxel-Resistant Phenotype. *Clin. Cancer Res.* **1999**, *5*, 3445−3453.
(39) Duan, Z.; Brakora, K. A.; Seiden, M. V. Inhibition of ABCB1 (MDR1) and ABCB4 (MDR3) Expression by Small Interfering Rna and Reversal of Paclitaxel Resistance in Human Ovarian Cancer Cells. *Mol. Cancer. Ther.* **2004**, *3*, 833−838.
(40) Gao, Y.; Foster, R.; Yang, X.; Feng, Y.; Shen, J. K.; Mankin, H. J.; Hornicek, F. J.; Amiji, M. M.; Duan, Z. Up-Regulation of CD44 in the Development of Metastasis, Recurrence and Drug Resistance of Ovarian Cancer. *Oncotarget* **2015**, *6*, 9313−9326.
(41) You, M.; Zhong, J.; Hong, Y.; Duan, Z.; Lin, M.; Xu, F. Inkjet Printing of Upconversion Nanoparticles for Anti-Counterfeit Applications. *Nanoscale* **2015**, *7*, 4423−4431.
(42) Feng, A. L.; You, M. L.; Tian, L. M.; Singamaneni, S.; Liu, M.; Duan, Z. F.; Lu, T. J.; Xu, F.; Lin, M. Distance-Dependent Plasmon-Enhanced Fluorescence of Upconversion Nanoparticles Using Polyelectrolyte Multilayers as Tunable Spacers. *Sci. Rep.* **2015**, *5*, 7779.
(43) Lee, S. K.; Han, M. S.; Asokan, S.; Tung, C.-H. Effective Gene Silencing by Multilayered siRNA-Coated Gold Nanoparticles. *Small* **2011**, *7*, 364−370.
(44) Song, W.-J.; Du, J.-Z.; Sun, T.-M.; Zhang, P.-Z.; Wang, J. Gold Nanoparticles Capped with Polyethyleneimine for Enhanced siRNA Delivery. *Small* **2010**, *6*, 239−246.
(45) Wu, S.; Duan, N.; Ma, X.; Xia, Y.; Wang, H.; Wang, Z. A Highly Sensitive Fluorescence Resonance Energy Transfer Aptasensor for Staphylococcal Enterotoxin B Detection Based on Exonuclease-

DOI: 10.1021/acsami.6b15321
ACS Appl. Mater. Interfaces XXXX, XXX, XXX−XXX

Catalyzed Target Recycling Strategy. *Anal. Chim. Acta* **2013**, *782*, 59−66.
(46) Wang, S.; Zhou, Y.; Niu, H.; Zhang, X. Layer-by-Layer Self-Assembly of Polyaspartate and Poly(Ethyleneimine) on Magnetic Nanoparticles: Characterization and Adsorption of Protein. *Curr. Appl. Phys.* **2011**, *11*, 1337−1342.
(47) Xu, Y.; Du, Y. Effect of Molecular Structure of Chitosan on Protein Delivery Properties of Chitosan Nanoparticles. *Int. J. Pharm.* **2003**, *250*, 215−226.
(48) Kowalik, K. M.; Shimada, Y.; Flury, V.; Stadler, M. B.; Batki, J.; Buhler, M. The PAF1 Complex Represses Small-RNA-Mediated Epigenetic Gene Silencing. *Nature* **2015**, *520*, 248−252.
(49) Hohng, S.; Lee, S.; Lee, J.; Jo, M. H. Maximizing Information Content of Single-Molecule Fret Experiments: Multi-Color Fret and Fret Combined with Force or Torque. *Chem. Soc. Rev.* **2014**, *43*, 1007−1013.
(50) Alabi, C. A.; Love, K. T.; Sahay, G.; Stutzman, T.; Young, W. T.; Langer, R.; Anderson, D. G. Fret-Labeled siRNA Probes for Tracking Assembly and Disassembly of siRNA Nanocomplexes. *ACS Nano* **2012**, *6*, 6133−6141.
(51) Mattsson, L.; Wegner, K. D.; Hildebrandt, N.; Soukka, T. Upconverting Nanoparticle to Quantum Dot Fret for Homogeneous Double-Nano Biosensors. *RSC Adv.* **2015**, *5*, 13270−13277.
(52) Pons, T.; Medintz, I. L.; Sapsford, K. E.; Higashiya, S.; Grimes, A. F.; English, D. S.; Mattoussi, H. On the Quenching of Semiconductor Quantum Dot Photoluminescence by Proximal Gold Nanoparticles. *Nano Lett.* **2007**, *7*, 3157−3164.

DOI: 10.1021/acsami.6b15321
ACS Appl. Mater. Interfaces XXXX, XXX, XXX−XXX